JOURNAL OF AIRCRAFT
Vol. 43, No. 4, July–August 2006

Combining Passive Control Method for Dynamic Stall Control

Wandon Joo*
Seoul National University, 313-317, Seoul 151-742, Republic of Korea
Bo-sung Lee†
Samsung SDS, Seoul 135-918, Republic of Korea
Kwanjung Yee‡
Pusan National University, Pusan 609-735, Republic of Korea
and
Dong-ho Lee§
Seoul National University, Seoul 151-742, Republic of Korea

To demonstrate the benefits of a combined nose droop and Gurney flap for improving dynamic stall and post-stall aerodynamic characteristics of a rotor airfoil, numerical investigations and design optimization have been performed. As a means of passive flow control, a fixed nose droop has been deliberately employed together with a Gurney flap. For shape optimization, droop location and droop angle were selected as design variables for the fixed nose droop, and the flap length was chosen as a design variable for the Gurney flap. Bousman's function plot was employed to define the objective function and constraint conditions. A feasible direction-based optimizer and a higher-order response surface method were harnessed to handle the highly nonlinear properties of dynamic stall. By the use of this methodology, optimum design was carried out to enhance lift and pitching moment characteristics simultaneously; at the same time, the unfavorable effects of the overall movement of the pitching moment coefficient induced by droop and the Gurney flap was reduced. It is also proved that by utilizing a 22.7-deg droop at the 0.275 chord droop position and a 1.14% chord Gurney flap, the stall can be delayed by a maximum lift coefficient increased by 13%, a maximum negative pitching moment reduced by 60%, and the lift-to-drag ratio increased accordingly. The present combined passive control methods and design result show significant improvement of aerodynamic performance in Bousman's plot in terms of lift and pitching moment.

Nomenclature

a_∞	=	speed of sound
C	=	airfoil chord
$C_{d\,\max}$	=	maximum drag coefficient
$C_{l\,\max}$	=	maximum lift coefficient
$C_{m\,\min}$	=	maximum negative pitching moment coefficient; minimum pitching moment coefficient
$C_{m\,\text{min-Dn}}$	=	minimum moment coefficient at downstroke
$C_{m\,\alpha\text{-min}}$	=	moment coefficient at minimum angle of attack
$\boldsymbol{E}, \boldsymbol{F}$	=	convective fluxes
$\boldsymbol{E}_v, \boldsymbol{F}_v$	=	viscous fluxes
J	=	Jacobian of transformation matrix
k	=	reduced frequency of oscillating airfoil motion, $\omega/2M_\infty$
M_∞	=	freestream Mach number
P	=	droop position, $1/4C - 1/16C \leqq P \leqq 1/4C + 1/16C$
$\boldsymbol{Q}$	=	vector of conservative variables
t	=	nondimensionalized physical time
x, y	=	Cartesian coordinate
α	=	angle of attack
θ	=	droop angle, $10 \leqq \theta \leqq 30$ deg
ξ, η	=	time-dependent curvilinear coordinates
ρ_∞	=	normalized density
ϕ	=	constraint condition
ω	=	frequency of oscillating airfoil motion

Presented as Paper 2005-1363 at the AIAA 43rd Aerospace Sciences Meeting and Exhibit, Reno, NV, 10–13 January 2005; received 30 May 2005; revision received 20 September 2005; accepted for publication 23 September 2005.

*Ph.D. Candidate, School of Mechanical and Aerospace Engineering; aerodon3@yahoo.co.kr. Member AIAA.
†Senior Consultant, Consulting Division, Office of Enterprise Resource Planning Consulting, 709-19 Yeoksam-2 Dong Gangnam-Gu; bosung.lee@samsung.com. Member AIAA.
‡Professor, Department of Aerospace Engineering; daedalus@pusan.ac.kr. Member AIAA.
§Professor, School of Mechanical and Aerospace Engineering; donghlee@snu.ac.kr. Member AIAA.

I. Introduction

DYNAMIC stall refers to a series of complicated aerodynamic phenomena associated with the delay of stall beyond the static stall angle of an airfoil due to the unsteady dynamic motion.[1] In most cases, dynamic stall induces an abrupt fluctuation of aerodynamic forces, resulting in the imposition of excessive structural load as well as control force. Hence, dynamic stall is considered the crucial factor limiting a helicopter's forward flight performance and aeroelastic stability of the wind-turbine blade. For the past decades, dynamic stall has been the one of the major problems of interest to helicopter and wind-turbine aerodynamicists; therefore, numerous studies have been focused on boosting the aerodynamic features of dynamic stall.

Various passive and active control methods have been suggested such as slat or slot,[2] suction, and blowing[3] to improve dynamic stall properties by suppressing the separation of an airfoil. Recently, Joo et al.[4] have tried a variable airfoil thickness concept as a means to enhance or modify the characteristics of dynamic stall. On the other hand, the forced buzzing of the leading-edge surface has been examined by Park et al.,[5] in which boundary-layer separation is controlled by supplying additional kinetic energy to the boundary layer. An oscillatory jet with zero-net-mass jet concept was also studied by Nagib et al.[6] and Ahmed et al.[7] with a view to enhancing the static and dynamic stall aerodynamic characteristics. An active flap, commonly used in fixed aircraft, has also been applied on rotor airfoils.[8] Through these various studies, it was found that dynamically deforming leading edge (DDLE)[9] and variable droop leading edge (VDLE)[10] methods are very effective for enhancing

the pitching moment characteristics of dynamic stall. In the case of DDLE, leading-edge curvature of the airfoil is dynamically changed. In the case of VDLE, the airfoil camber is changed by a dynamic leading-edge droop. However, their effects were nearly the same. Both controlled dynamic stall by controlling the vorticity flux over the airfoil.

Most of the previous passive stall control methods, however, were not so successful in simultaneously improving lift and pitching moment characteristics of dynamic stall, mainly because lift variation has the opposite characteristics of the pitching moment variation. In other words, the improvement of lift characteristics causes the deterioration of pitching moment characteristics and vice versa. To overcome this problem of the control method, Chandrasekhara et al.[11] drew on a combination of a Gurney flap in conjunction with VDLE. The effectiveness of VDLE on dynamic stall is that a significant improvement of moment performance was realized and was proven in Ref. 12. On the other hand, the Gurney flap[13,14] has been adopted as a stabilizer to fixed-wing aircraft and racing cars for the purpose of enhancing dynamic characteristics. Even though it is very easy to apply, it is known to be effective for increasing lift by over 20%. The combined use of a VDLE with a Gurney flap is shown in Ref. 11. Lift characteristics were raised satisfactorily with significant improvement of pitching moment characteristics. Despite this impressive improvement of dynamic stall performance, active control methods have intrinsic problems in that they require an auxiliary mechanical device that takes up space in a rotor blade. Therefore, it seems difficult implement on an actual helicopter or wind turbine at present.

Hence, a combination of a Gurney flap in conjunction with a fixed droop leading edge (FDLE) has been applied to the control of dynamic stall to solve concurrently the aforementioned problems. That is, the FDLE is expected to improve pitching moment characteristics, while the gurney flap is supposed to improve lift characteristics at the same time. However, a FDLE has an unfavorable projection effect, even though easier to realize than a VDLE. As a result, drag performance is slightly lower than baseline airfoil at a low angle of attack.[12] To mitigate this disadvantage and find the optimal combination of both devices, a design optimization was conducted. Because a simple combination of the two aforementioned devices may not guarantee successful improvement in the dynamic stall characteristics it is anticipated that, through a design process, an optimized combined passive control device can be found and placed after an active control device such as VDLE.

For design optimization, a higher-order response surface methodology (RSM)[15] and feasible direction-based optimizer were mobilized. In the case of unsteady and nonlinear problems such as dynamic stall, a substantial amount of time and cost will be required for numerical analysis. Hence, RSM can be an effective tool in the design process, and the feasible direction-based optimizers are known to be adequate for a well-posed RSM. DOT[16] was used for optimization.

The present research consists of two parts: 1) the numerical investigation of dynamic stall characteristics with respect to each control method and 2) the design optimization of each passive control method for a best combination effect. Also, a primary advantage may be that the present concept is viable for actual realization.

II. Governing Equations and Numerical Implementation

The governing equations for an unsteady flowfield in conservative form are written as in Eq. (1) by introducing a general curvilinear coordinate system $\xi = \xi(t, x, y)$ and $\eta = \eta(t, x, y)$,

$$\frac{1}{J}\frac{\partial Q}{\partial t} + \frac{\partial E}{\partial \xi} + \frac{\partial F}{\partial \eta} = \frac{\partial E_v}{\partial \xi} + \frac{\partial F_v}{\partial \eta} \tag{1}$$

In Eq. (1), $\boldsymbol{Q}$ represents conservative variables, and $\boldsymbol{Q}$ is $[\rho, \rho u, \rho v, \rho e, k, \omega]^T$ in the two-dimensional problem. $\boldsymbol{E}$ and $\boldsymbol{F}$ are convection terms, and $\boldsymbol{E}_v$ and $\boldsymbol{F}_v$ are viscous terms. T is physical time and $J = \xi_x\eta_y - \eta_x\xi_y$ stands for the transformation Jacobian. All geometric variables are nondimensionalized separately, by airfoil chord length C, density ρ by freestream density ρ_∞, and velocity u and v by speed of sound a_∞.

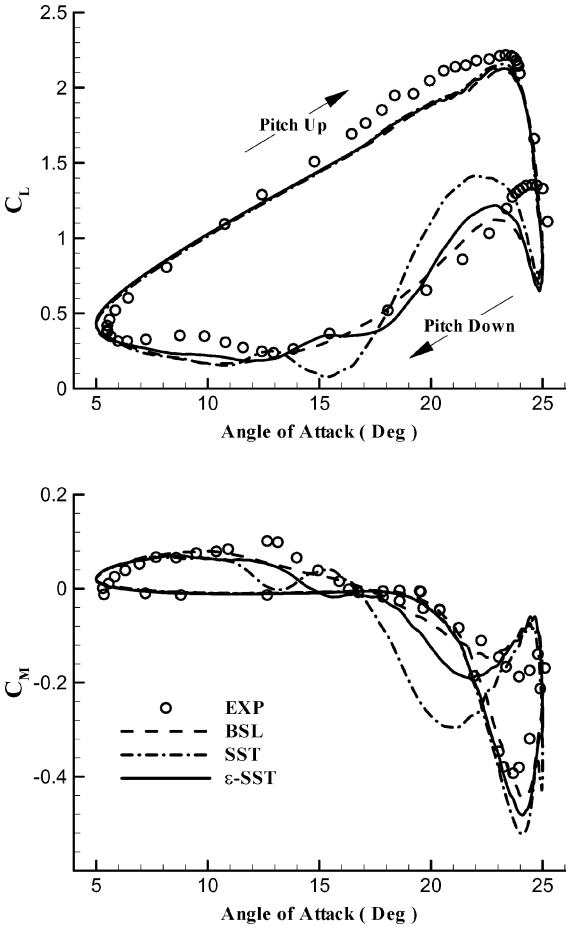

Fig. 1 Hysteresis effects for deep stall obtained with three models: NACA0012, $M_\infty = 0.283$, $Re = 3.45 \times 10^6$, $\alpha(t) = 15\text{ deg} + 10\text{ deg}\sin(\omega t)$, and $k = 0.151$.

A dual time-stepping method has been tapped to obtain higher-order temporal accuracy for unsteady flowfields. Roe's flux difference scheme is used for spatial discretization of inviscid terms, whereas the central difference scheme is reserved for the discretization of viscous terms. Computation time has been greatly reduced through parallel computing for which the data parallel symmetric Gauss–Seidel (DP-SGS)[17] method and domain decomposition method are used. For the case of turbulence, the ε–SST[18] turbulence model, modified from Menter's SST model, is used to improve separated flowfields.

First, numerical analysis is executed for a NACA0012 airfoil and is compared with experimental results. Pitch angle is varied as $\alpha(t) = 15\text{ deg} + 10\text{ deg}\sin(\omega t)$, and the reduced frequency k is 0.151. The freestream Mach number is 0.283, and the Reynolds number is set as 3.45×10^6 as in the experiment.[19]

For an unsteady calculation, each period is divided by 1440 physical time steps. After a converged solution is obtained at each time step, physical time is advanced to the next step by a dual time-stepping method. Figure 1 shows the variation of aerodynamic coefficients during one period. Although stall angle and the angle of reattachment after stall are in good agreement with experiments, the maximum values of coefficients are shown to be somewhat different than those of experiments.

III. Dynamic Stall Control Methods

As indicated in Bousman's plot[20] in Fig. 2, most of the dynamic stall control methods fail to improve both lift and pitching moment characteristics. Note that nose droop eliminates or alleviates separation by modifying the inflow angle at the airfoil's droop section,

where inflow angle is retained at the airfoil's nondroop section. In contrast, the trailing-edge flap and cambered airfoil are known to have the opposite characteristics. As mentioned earlier, Martin et al.[10] showed that the application of variable nose droop can enhance the pitching moment characteristics while retaining the reasonable lift performance, as shown in Fig. 2. However, the actual objective of rotor airfoil design is to improve concurrently lift and pitching moment characteristics. In other words, the aerodynamic characteristics of the designed airfoil should move toward the first quadrant of the Bousman plot. In this regard, the present study is designed to achieve this goal by combining the two different control methods simultaneously. Figure 3 shows schematically the basic concepts of the present approach that simultaneously employs a nose droop and Gurney flap among various passive control methods.

As shown in Fig. 3, fixed nose droop has been applied in the present study for the purpose of improving pitching moment characteristics of a rotor airfoil. It is known to delay the separation at a high angle of attack. However, fixed nose droop has a tendency to degenerate lift characteristics at low angles of attack. In addition, as can be found in an other experiment,[12] the drag may increase at near a zero angle of attack due to the projection of the drooped nose.

The Gurney flap, first applied by D. Gurney (see Refs. 13 and 14), is a high-lift device, vertically attached on trailing edge of an airfoil with 1–4% of airfoil chord length. Although very simple to implement, it is significantly effective in increasing lift. Because of this feature, the Gurney flap has been selected as a horizontal stabilizer of an aircraft or a spoiler of racing car to improve stability. Figure 3 shows the typical configuration of a Gurney flap and the flowfields around it. Note from Fig. 3 that small separation bubbles are generated at the front and back of Gurney flap, increasing circulation around airfoil. Lift of an airfoil increases by the amount of the increase of circulation, but other aerodynamic coefficients such as drag and pitching moment are increased as well.

In this section, the static and dynamic stall characteristics of each flow control method are investigated for a NACA0012 airfoil.

A. Static Stall Characteristics

A series of numerical calculations for static stall has been performed for a NACA0012 airfoil with a nose droop and Gurney flap, respectively. The aerodynamic coefficients are compared for baseline airfoil, fixed nose droop of 20 deg, 0.5%C Gurney flap, and the combination of both as shown in Fig. 4. The freestream Mach number is set as 0.283, and Reynolds number based on airfoil chord length is 3.45×10^6.

In Fig. 4, aerodynamic coefficients with angle of attack are shown for each case. It is found that the static stall angle and drag divergence are delayed for the airfoil with a 20-deg fixed nose droop. However, the mean lift is lower than that of the baseline airfoil at a lower angle of attack. For the single application of a 0.5%C Gurney flap, the static stall and drag divergence occur earlier than baseline airfoil. However, with the combination of a 20-deg fixed nose droop with a 0.5%C Gurney flap, lift increases and drag divergence as well as static stall are, in turn, delayed. The combination of the fixed nose droop with a Gurney flap not only enhances lift and drag performance, but the pitching moment is also significantly reduced. In this vein, the lift-to-drag ratio is better than that of baseline airfoil at the overall angle of attack. From the static stall calculation,

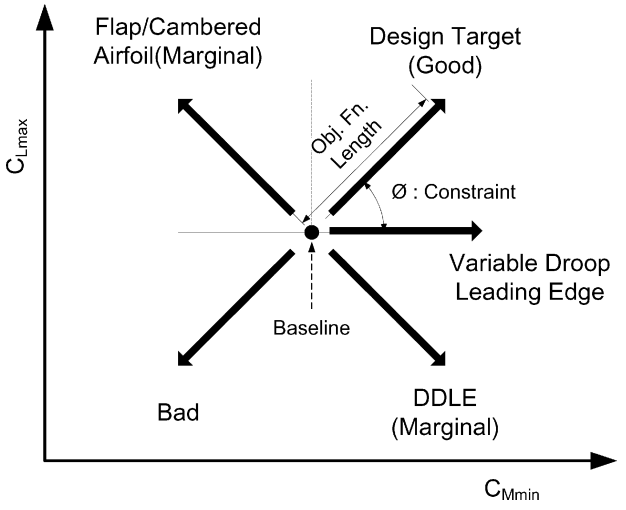

Fig. 2 Bousman's dynamic stall function plot.[20]

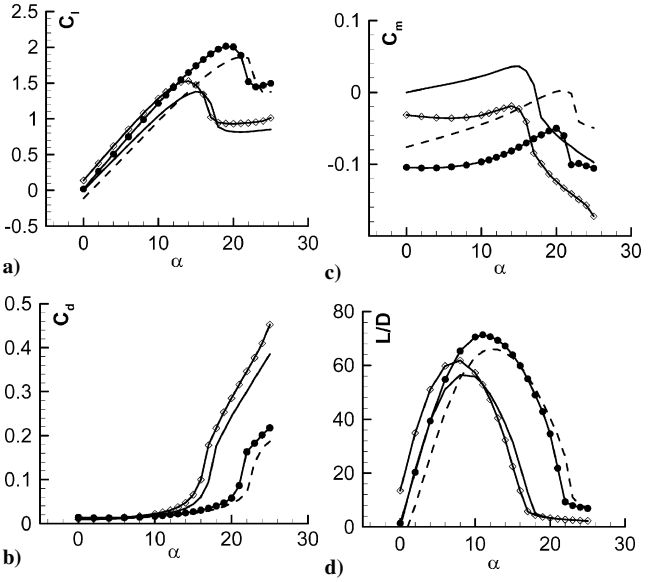

Fig. 4 Static aerodynamic properties: a) quasi-static lift coefficient, b) drag coefficient, c) moment coefficient, and d) lift-to-drag ratio vs angle of attack according to different control schemes: ——, NACA0012 baseline; – – –, 20-deg, fixed droop; ◇, 0.5%C gumey flap; and ●, 20-deg, fixed droop and 0.5%C gumey flap.

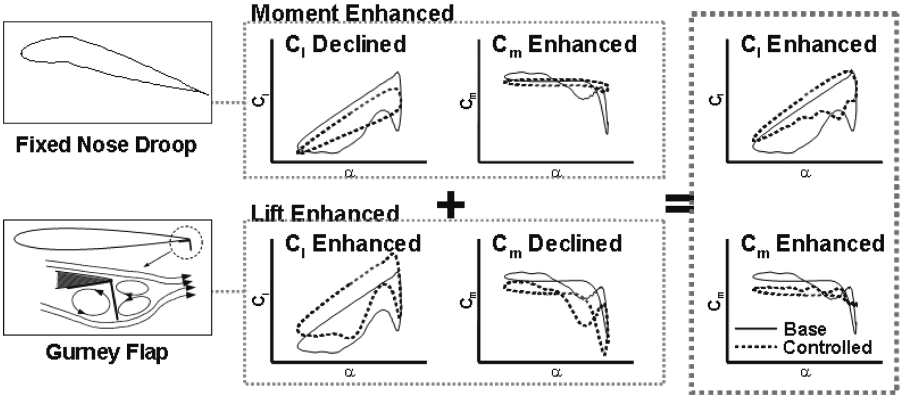

Fig. 3 Schematic diagram of control scheme.

it is shown that the overall aerodynamic performances are greatly enhanced with the combination of two passive control devices.

B. Dynamic Stall Characteristics

A series of numerical calculations for dynamic stall has been followed with various angles of nose droop and sizes of Gurney flap. The pitch angle variation follows $a(t) = 15 \text{ deg} + 10 \text{ deg} \sin(\omega t)$, where k is the reduced frequency of 0.151, the freestream Mach number is 0.283, and the Reynolds number is 3.45×10^6, as in the experiment.[19] First, flowfields around a NACA0012 airfoil with a fixed nose droop of 10, 15, and 20 deg have been studied. Second, Gurney flaps with sizes of 0.5%, 1%, and 1.5% of chord of the baseline NACA0012 airfoil have been applied. Finally, both fixed nose droop and Gurney flap are simultaneously applied to the baseline airfoil.

Figure 5 shows calculation results of fixed nose droop. In Fig. 5, the absolute values of $C_{m\,\min}$ and $C_{d\,\max}$ are reduced with the increase in droop angle, whereas the $C_{l\,\max}$ retains those of baseline airfoil. However, the increase of droop angle has a tendency to increase the overall pitching moment level in the negative direction in spite of a remarkable reduction of the maximum negative pitching moment coefficient.

Figure 6 shows the results of the application of a Gurney flap to the NACA0012 airfoil. Note from Fig. 6 that lift increases with the size of Gurney flap, whereas the maximum drag and pitching moment characteristics are getting worse. For the case of a 1.5%C Gurney flap, it is observed that the maximum lift is increased by about 25%.

As expected, fixed nose droop is shown to be effective in improving pitching moment characteristics but induces negative results in lift, whereas the Gurney flap shows the opposite characteristics. Pitching moment characteristics may be expected to be improved by fixed nose droop, whereas the Gurney flap will have a favorable effect on the lift. Based on this concept, a numerical simulation is conducted in this study to verify the benefits of the current concept.

Figure 7 shows the numerical results of a fixed nose droop with a Gurney flap, where the droop angle is fixed at 20 deg and the Gurney flap sizes vary from 0.5 to 1.5% of the airfoil chord length. The 0.5%C Gurney flap with 20-deg nose droop yields the best results. At the same time, drag level is significantly reduced, compared with that of baseline airfoil. It is concluded that by deliberate combination of Gurney flap with nose droop, the control objective can be effectively achieved. In addition, the present concept has an advantage of simple implementation in comparison with other active control methods.

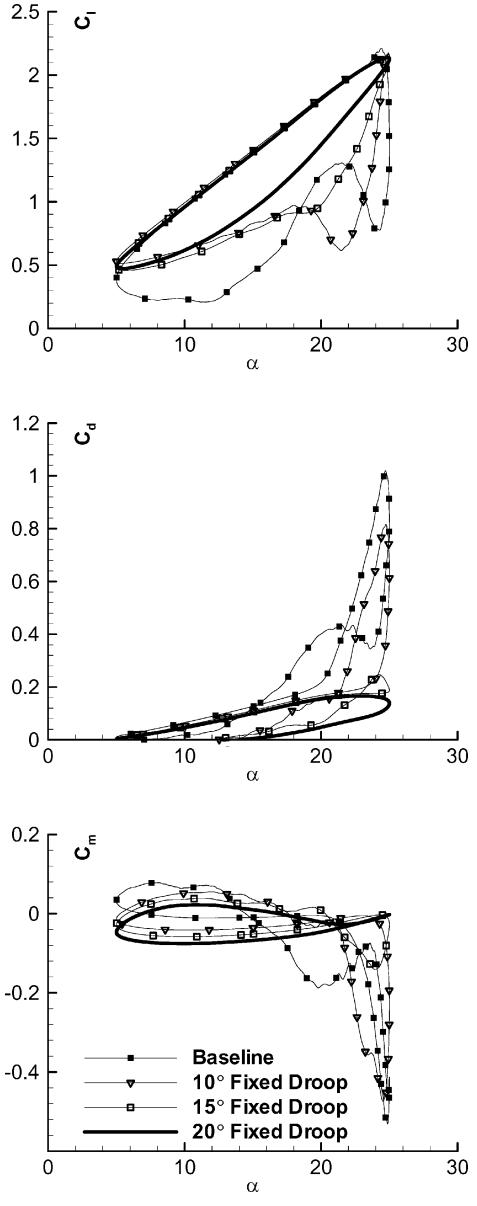

Fig. 5 Hysteresis effects with fixed nose droop: $M_\infty = 0.283$, $Re = 3.45 \times 10^6$, $\alpha(t) = 15 \text{ deg} + 10 \text{ deg} \sin(\omega t)$, and $k = 0.151$.

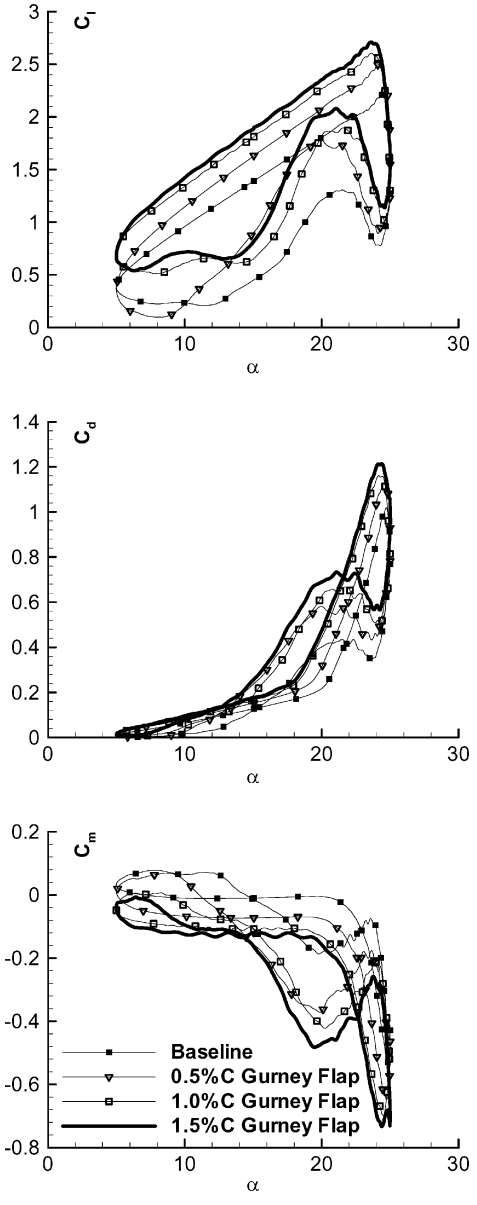

Fig. 6 Hysteresis effects with Gurney flap: $M_\infty = 0.283$, $Re = 3.45 \times 10^6$, $\alpha(t) = 15 \text{ deg} + 10 \text{ deg} \sin(\omega t)$, and $k = 0.151$.

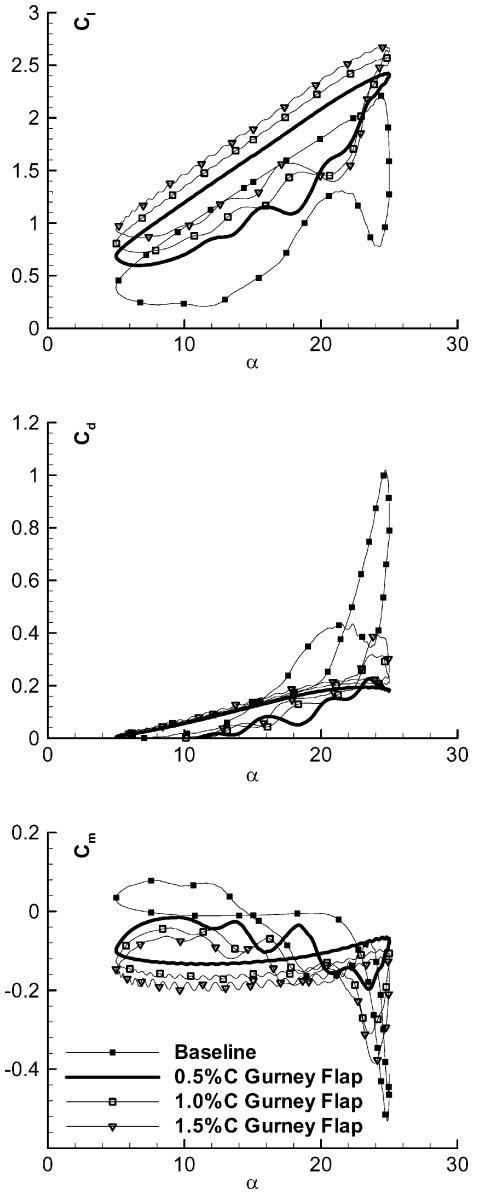

Fig. 7 Hysteresis effects with combination of fixed nose droop and Gurney flap: $M_\infty = 0.283, Re = 3.45 \times 10^6, \alpha(t) = 15\,\text{deg} + 10\,\text{deg}\sin(\omega t)$, and $k = 0.151$.

The flowfield around an airfoil with a 0.5%C Gurney flap with a 20-deg nose droop at its maximum pitch angle is shown in Fig. 8. Note that in the baseline airfoil, as the pitch angle increases, the leading-edge vortex propagates along the airfoil surface. During the downstroke, a secondary vortex develops at the rear of the airfoil and moves upstream. On the other hand, trailing-edge stall is discerned for the airfoil with the combination of a nose droop and Gurney flap. As is well known, the vortex intensity for trailing-edge stall is relatively weak, resulting in the increase of a minimum pitching moment. It is also shown that during the downstroke reattachment occurs earlier than in the case of the baseline, which produces the early recovery of lift.

IV. Design Optimization

A. Design Variables

Droop angle and its position were chosen as the main design variable for determining the characteristics of the droop. As mentioned in the preceding section, droop tends to increase overall pitching moment level in the negative direction in spite of a remarkable reduction of the maximum negative pitching moment coefficient. For this unfavorable effect of droop angle, additional design variables were

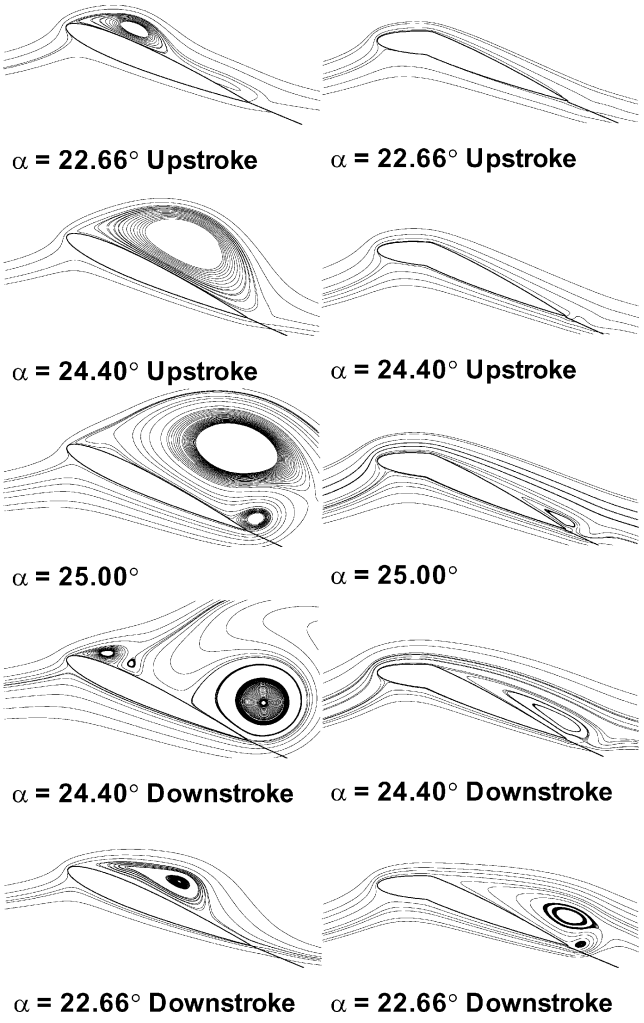

Fig. 8 Instantaneous streamline distributions of various angle of attack: a) baseline airfoil and b) 20-deg fixed nose droop with 0.5%C Gurney flap.

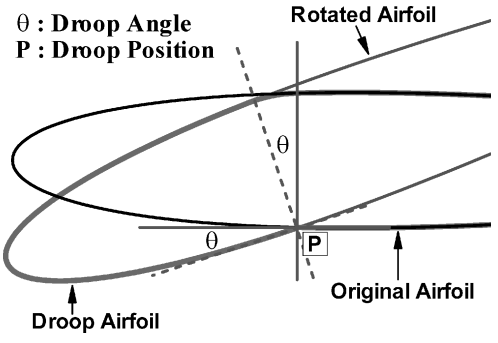

Fig. 9 Design variables of fixed nose droop (position and angle).

introduced to compensate the effects of droop angle. Figure 9 shows the two design variables of a fixed nose droop. Droop was set by rotating the front of the leading edge of the base airfoil (NACA0012) about the droop position P by droop angle θ. Note that the surface of the upper airfoil must be induced by droop, and, to produce a smooth surface, a spline function needs to be applied.

The height of Gurney flap was selected as the design variable of the Gurney flap. The height can vary from 0 to 2% of the chord length. The specification of design variables is listed in Table 1.

B. Parameters of Dynamic Stall

It is desirable to define clearly the parameters of dynamic stall that dominate the characteristics of each control method. Parameters

Table 1 Specification of design variables

Design variable	Lower bound	Upper bound
	Droop	
Position, P	$1/4C - 1/16C$	$1/4C + 1/16C$
Angle θ, deg	10	30
	Gurney flap	
Height	0%C	2%C

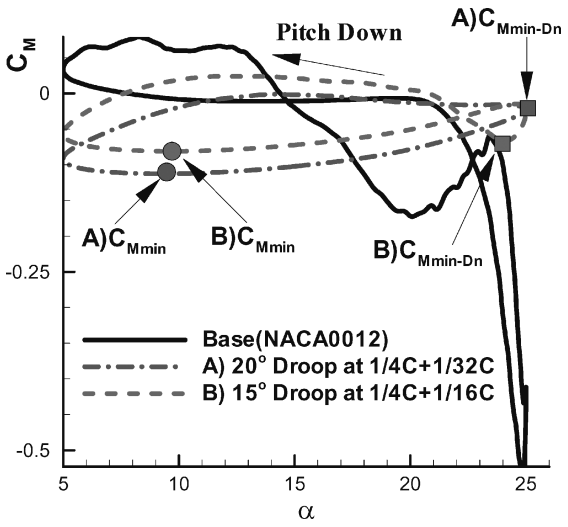

Fig. 10 With and without negative damping case.

for dynamic stall characteristics are stall angle, maximum lift coefficient, maximum negative pitching moment, negative damping area, drag divergence angle, maximum drag coefficient, etc. Because each passive control method has a compound effect on these aerodynamic coefficients, it is important to have a good understanding of the correlation between each control method and the aerodynamic coefficients.

Three aerodynamic coefficients are considered to represent the effects of control methods. 1) maximum lift coefficient, 2) moment coefficient at pitchdown, and 3) moment coefficient at minimum angle of attack.

1) For maximum lift coefficient $C_{l\max}$, it is observed that the Gurney flap improves the lift performance but has an unfavorable effect on the pitching moment characteristics due to the excessive moment stall. In contrast, the droop has no significant effect on the lift and primarily affects the moment performance. Thus, maximum lift coefficient is selected as the parameter to indicate the lift performance brought about by the Gurney flap.

2) For the moment coefficient of pitchdown $C_{m\,\text{min-Dn}}$, when the effect of droop grows, the maximum negative pitching moment may not represent the moment characteristics. For example, in case A of Fig. 10, negative damping doesnot exist because dynamic stall doesnot occur, whereas negative damping exists due to dynamic stall in case B of Fig. 10. Notwithstanding, with the investigation of the moment of case A for one cycle, the moment for pitchup motion was chosen as the maximum negative pitching moment, and so it seems to have a worse moment characteristic. When the effect of droop grows, the growth of the maximum negative pitching moment by dynamic stall is suppressed, but the overall increase of the moment characteristic occurs at the entire region of airfoil oscillation. Because of this, the maximum negative pitching moment during one cycle sometimes has nothing to do with the existence of the negative damping area.

From the viewpoint of structure and control, the existence of the negative damping area is one of the worst characteristics. Therefore, to represent the moment characteristic using a maximum negative pitching moment, it should be defined at specified range of angle of attack. For this, the maximum moment coefficient of pitch-down is chosen as the parameter that represents the moment characteristic. However, as in the case of the baseline NACA0012, dynamic stall arise before pitchdown starts. To examine this, the maximum moment is defined from 23 deg, which is before the maximum pitchup angle.

3) For the moment coefficient at a minimum angle of attack $C_{m\,\alpha\text{-min}}$, the preceding section shows that overall pitching moment level moves to in the negative direction when the droop angle increases. To consider this characteristic of the design of droop, it is necessary to define the variable that can indicate the overall movement of the moment coefficient. The overall movement of the moment coefficient shall be seen as the geometrical effect of droop rather than the change in the coefficient caused by the dynamic stall itself. Thus, it is desirable to take a value of the moment coefficient at a steady-state flowfield. For this reason, we defined moment coefficients at a minimum angle of attack that indicates the overall movement of the moment coefficient by droop.

C. Definition of Objective Function and Constraints

Bousman's dynamic stall function,[20] expressed in maximum lift coefficient $C_{l\max}$ and minimum pitching moment coefficient $C_{m\min}$ is the most representative method of displaying dynamic stall characteristics. As shown in Fig. 2, the design result should be located on the first quadrant of the Bousman dynamic stall function to improve lift and moment coefficient simultaneously. In addition, the overall movement of the pitching moment is minimized to prevent additional moment force in the airfoil's oscillating motion due to droop. The objective function (maximized) was defined as shown hereafter to meet these conditions using the performance parameter mentioned in the preceding section:

$$\text{wt} \times \sqrt{(C_{l\max} - C_{l\,\text{max-}B})^2 + (C_{m\,\text{min-Dn}} - C_{m\,\text{min-Dn-}B})^2} - (1 - \text{wt}) \times |C_{m\alpha\text{-min-}B} - C_{m\alpha\text{-min}}| \tag{2}$$

The square root term of the objective function is a condition intended to maximize the distance between the design value and baseline in Bousman's dynamic stall function plot. The second term is a condition to minimize the difference of the pitching moment at a minimum angle of attack and the baseline value. The final objective function adopts weight function wt. When the weight function is 1.0, only the distance in Bousman's dynamic stall function is maximized, and when the weight function is 0.5, it additionally minimizes the reduction in the pitching moment at the minimum angle of attack.

Constraint is defined as the angle ϕ that the design value has about the baseline value in Bousman's dynamic stall function plot, subject to

$$0 \leqq \phi \leqq 90 \text{ deg}$$

$$\phi = \tan^{-1}[(C_{l\max} - C_{l\,\text{max-}B})/(C_{m\min} - C_{m\,\text{min-}B})] \tag{3}$$

Constraint ϕ is set to range between 0 and 90 deg. This means that coefficients of maximum lift and maximum negative pitching moment at the downstroke must be better than those of the NACA0012 base airfoil because the design result should be in the first quadrant of Bousman's dynamic stall function plot. When the constraint condition ϕ is 0, the pitching moment is optimized, whereas when the ϕ is 90, the lift is optimized. In addition, the lift and the moment characteristics can be improved by adjusting the constraint condition ϕ.

Note that the lift and moment characteristics may not show similar levels of improvement. If the constraint condition ϕ is calculated using the normalized values of the baseline, it may be possible to improve lift and moment characteristics by the same ratio. In this case, the improvement ratio of the lift and moment coefficients will be limited to a relatively small one. Accordingly, the enhancement of moment performance shall be limited to the extent of the improvement rate of lift.

Table 2 R^2_{adj} of response surface models with polynomial's order[a]

Order of polynomial	R^2_{adj}				
	$C_{l\,max}$	$C_{d\,max}$	$C_{m\,min}$	$C_{m\,min\text{-}Dn}$	$C_{m\,\alpha\text{-}min}$
Second (15 pts)	0.996	0.957	0.896	0.881	0.997
Third (30 pts)	0.996	0.966	0.952	0.952	0.997
Fourth (50 pts)	0.997	0.990	0.981	0.981	0.998

[a]DOE (*D*-Opt).

D. Design Methodology

RSM[15] is a representative approximation method used to find a global optimum. In general, the response surface is organized in a second-order polynomial expression of a design variable used in optimizing. However, in the present study, the fourth-order polynomial response surface and feasible direction-based optimizer DOT[16] were used in the optimization process. Because the aerodynamic performance parameter of dynamic stall has a tendency foward highly nonlinear characteristics, accordingly, dynamic stall may or may not occur.

An accurate response surface is of great significance for reliable design results, and the confidence level of polynomial response model has been determined with regression analysis and analysis of variance. The regression analysis, R^2_{adj}, which is a measure of confidence regarding the organized response surface model, is represented as follows:

$$R^2_{adj} = 1 - [SS_E/(n-p)]/[S_{yy}/(n-1)] \tag{4}$$

In Eq. (4), SS_E is the sum of the error squared, S_{yy} is the sum of response function square value, n is the number of experimental points, and p is the number of the polynomial term.

Table 2 shows the R^2_{adj} of the aerodynamic performance parameter in terms of the order of response surface. As shown in Table 2, the second-order polynomial response surface of the minimum pitching moment at downstroke fails to satisfy the reasonable R^2_{adj}. For this reason, in this research, the fourth-order polynomial of the response surface model was used.

The design of the experiment was composed using the *D*-optimality[21] for constructing the response surface. It is generally known that *D*-optimality scheme is efficient enough to generate a response surface model with an optimum number of experiments. Table 2 shows the R^2_{adj} in accordance with the polynomial order of the response surface model. The second-order of polynomial could not result in a reasonable R^2_{adj}. For this reason, the fourth-order polynomial response surface model was used to improve the accuracy of the response surface in approximation.

The optimization was performed by applying the objective function and constraint condition with a consistent response surface model. Feasible direction-based optimization code DOT[16] was used for optimization.

V. Optimization Results

A total of four optimizations were carried out with respect to the change of objective function and the constraint condition. The results of each design and numerical analysis are shown in Table 3 and Fig. 11, respectively.

In case 1, the constraint condition ϕ was set to zero to maximize the moment characteristics only. It is found that the lift characteristic, similar to the NACA0012 baseline airfoil, showed a decrease in the maximum negative pitching moment (minimum pitching moment) of 72% and that no negative damping area could be observed. As can be seen in Fig. 11, the dynamic stall has been completely removed.

In case 2, the constraint condition ϕ is set to 90 to maximize the lift characteristics only. Whereas the maximum lift coefficient increased by 24% as shown in Fig. 11, the maximum negative pitching moment did not show any improvement and showed the another undesirable characteristics, that is, the growth of negative damping could be seen.

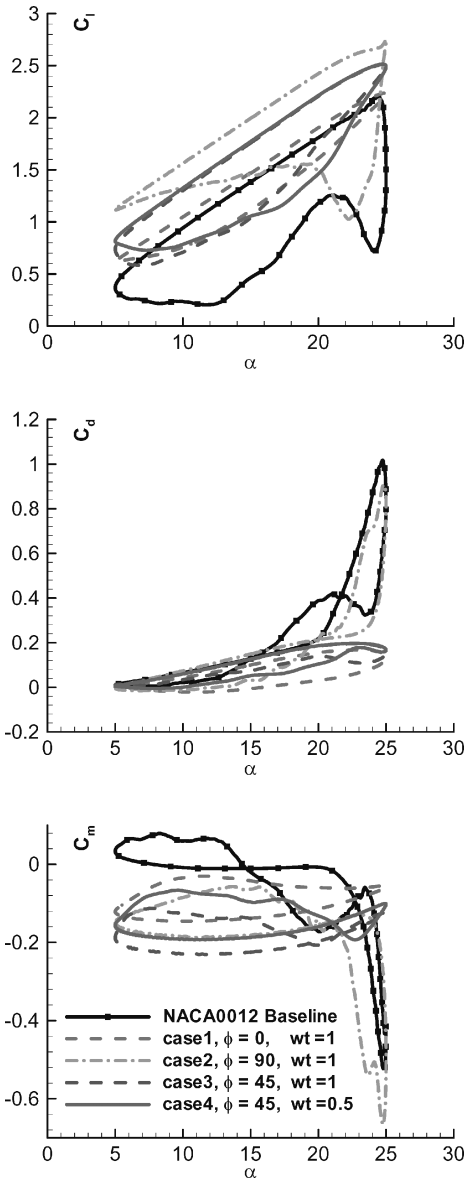

Fig. 11 Hysteresis of designed cases: $M_\infty = 0.283$, $Re = 3.45 \times 10^6$, $\alpha(t) = 15$ deg + 10 deg sin(ωt), and $k = 0.151$.

In case 3, it is attempted to improve simultaneously both lift and moment characteristics by setting the constraint condition ϕ to 45. The maximum lift coefficient increased by 14%, maximum negative pitching moment is improved by 56%, and the negative damping area is decreased by 98%. From Fig. 11, it could be confirmed that the performance of lift and moment characteristics were simultaneously elevated due to the effective control of the dynamic stall. However, the overall pitching moment could be seen to shift entirely in the negative direction, thereby causing the airfoil placed under a continuous pitching moment throughout the region. There may be a possibility of structural problems such as flutter when it is adapted to the rotor blade.

In case 4, the weight function was set to 0.5 for two purposes. One is to improve lift and moment characteristics simultaneously. The other is to prevent the overall increase of pitching moment by the droop and Gurney flap. Although the characteristics of lift, drag, and moment are similar to case 3, overall movements of pitching moment in the negative direction were reduced by minimizing pitching moment at a minimum angle of attack. This clearly showed that the fixed droop and Gurney flap were optimized to maximize their performance with a given condition, minimizing disadvantages. This finding may offer a good guideline to adapt fixed leading-edge droop and a Gurney flap on the rotor blade.

Table 3 Optimized design variables and performance with constraints

Parameter	Case 1	Case 2	Case 3	Case 4	Case 5
wt	1	1	1	0.5	——
ϕ, deg	0	90	45	45	——
Droop angle, deg	30.000	15.761	30.000	22.6713	——
Droop position	0.2554C	0.2409C	0.2738C	0.2751C	——
Gurney flap length	0.2105%C	2.0000%C	1.3794%C	1.1416%C	——
$C_{l\,\max}$	2.2372, 1%↑	2.7430, 24%↑	2.5138, 14%↑	2.5141, 13%↑	2.2125
$C_{m\,\min}$	−0.1456, 72%↑	−0.6668, −27%↓	−0.2309, 56%↑	−0.2087, 60%↑	−0.5231
$C_{d\,\max}$	0.1670, 84%↑	0.9071, 11%↑	0.1953, 81%↑	0.1970, 81%↑	1.0172
$C_{m\,\alpha\text{-min}}$	−0.1211	−0.1498	−0.1880	−0.1563	0.0336
$C_{m\,\text{min-Dn}}$	−0.1211	−0.6668	−0.2070	−0.1930	−0.5231
Negative damping area	0, 100%↑	55.101, −184%↓	0.3875, 98%↑	6.964, 64%↑	19.395

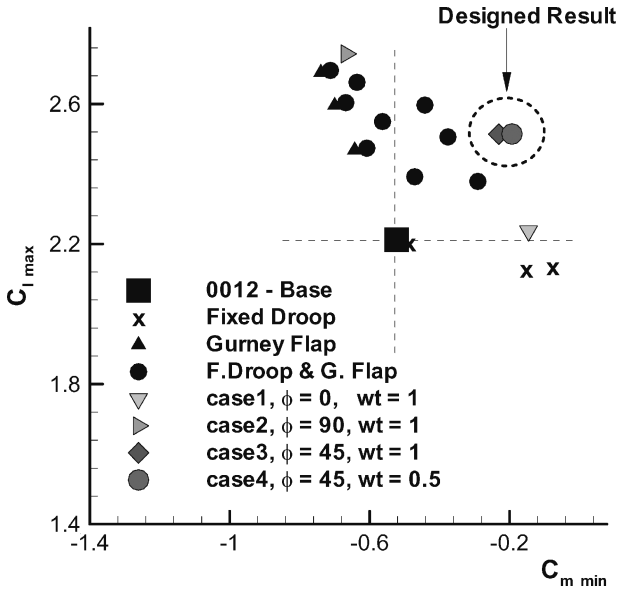

Fig. 12 Bousman's plot with optimized case of Gurney flap and fixed nose droop.

We compared the aforementioned cases with the case of separately used devices in Bousman's plot as shown in Fig. 12. Optimization findings show simultaneous improvement of lift and pitching moment performance. Furthermore, by adjusting the constraint condition design, a result can be located with a specific direction in the plot.

VI. Conclusions

The primary objective of the present study is to control and enhance the dynamic stall characteristics of a rotor airfoil by deliberately drawing on existing passive control methods. Among the existing control methods, fixed nose droop and a Gurney flap have been chosen and simultaneously applied to a NACA0012 airfoil, and design optimizations of each control method were performed. Feasible direction-based code DOT and a fourth-order polynomial response surface model were used in the design process to consider nonlinear characteristics of dynamic stall. The objective function used a weighting function to apply the condition of maximizing distance between the design and base results in Bousman's function plot and to minimize the overall movement of the pitching moment. Through the numerical investigation of the control methods and design optimization, we can draw the following conclusions:

1) By the deliberate combination of a Gurney flap and nose droop, enhancement of lift and pitching moment characteristics in dynamic stall can be achieved.

2) Fixed droop and the Gurney flap have been optimized to maximize their performance with a condition, minimizing disadvantages. This optimization process may be a good guideline to adapt fixed leading-edge droop and a Gurney flap on the rotor blade of a helicopter or wind turbine.

3) Through optimization, when applying 22.7 deg of droop angle at 0.275 chord and 1.14%C Gurney flap, the maximum lift coefficient increased by 13%, the maximum negative pitching moment decreased by 60%, and the negative damping area was reduced by 64% compared with the base airfoil.

4) The present passive control method can be easily applied to the rotor blade on account of its simplicity.

5) Finally, an investigation should be made of the compressibility effect on the advancing side of a rotor and aeroelastic stability, and experiments should be conducted for real applications.

Acknowledgments

The authors acknowledge support from the Korea Institute of Science and Technology Information under the Seventh Strategic Supercomputing Support Program. The use of the computing system of the Supercomputing Center is also greatly appreciated. We also gratefully acknowledge the grant from the Brain Korea 21 Project in 2005.

References

[1]Seddon, J., *Basic Helicopter Aerodynamics*, Blackwell Science, SW, Washington, 1990, Chap. 6.

[2]Plantin De Hugues, P., McAlister, K. W., and Tung, C., "Effect of an Extendable Slat on the Stall Behavior of a VR-12 Airfoil," NASA TP-3407, Sept. 1993.

[3]Ahn, T., Kim, C., and Rho, O., "Dynamic Stall Control Based on an Optimal Approach," *Journal of Aircraft*, Vol. 41, No. 5, 2004, pp. 1106–1116.

[4]Joo, W., Yee, K., Lee, B., and Lee, D., "Numerical Investigation of Dynamic Stall Control via Thickness Variation," *Journal of Aircraft*, Vol. 39, No. 2, 2002, pp. 262–270.

[5]Park, Y. W., Lee, S., Lee, D., and Hong, S., "Stall Control with Local Surface Buzzing on a NACA 0012 Airfoil," *AIAA Journal*, Vol. 39, No. 7, 2001, pp. 1400–1402.

[6]Nagib, H., Greenblatt, D., Kiedaisch, J., Wygnanski, I., and Hassan, A., "Effective Flow Control for Rotorcraft Applications at Flight Mach Numbers," AIAA Paper 2001-2974, June 2001.

[7]Hassan, A., Nagib, H., Wygnanski, I., "Oscillatory Jets—Benefits and Numerical Modeling Issues," *Proceedings of the 58th Annual Forum of the American Helicopter Society*, American Helicopter Society, Alexandria, VA, June 2002.

[8]Geissler, W., Sobieczky, H., Vollmers, H., "Numerical Study of the Unsteady Flow on a Pitching Airfoil with Oscillating Flap," *Proceedings of the 24th European Rotorcraft Forum*, Paper AE09, Sept. 1998.

[9]Chandrasekhaara, M. S., Wilder, M. C., and Carr, L. W., "Design and Development of a Dynamically Deforming Leading Edge Airfoil for Unsteady Flow Control," *Proceedings of the International Congress on Instrumentation in Aerospace Simulation Facilities*, Sept.–Oct. 1997, pp. 132–140.

[10]Martin, P. B., McAlister, K. W., Chandrasekhara, M. S., and Geissler, W., "Dynamic Stall Measurements and Computations for a VR-12 Airfoil with a Variable Droop Leading Edge," *Proceedings of the 59th Annual Forum of the American Helicopter Society*, American Helicopter Society, Alexandria, VA, May 2003.

[11]Chandrasekhara, M. S., Martin, P. B., and Tung, C., "Compressible Dynamic Stall Performance of a Variable Droop Leading Edge Airfoil with a Gurney Flap," AIAA Paper 2004-41, Jan. 2004.

[12]Chandrasekhara, M. S., Martin, P. B., and Tung, C., "Compressible Dynamic Stall Control Using a Variable Droop Leading Edge Airfoil," AIAA Paper 2003-48, Jan. 2003.

[13]Date, J. C., and Turnock, S. R., "Computational Evaluation of the Periodic Performance of a NACA0012 Fitted With a Gurney Flap," *Journal of Fluids Engineering*, Vol. 124, 2002, pp. 227–234.

[14]Houghton, E. L., and Carpenter, P. W., *Aerodynamics for Engineering Students*, Butterworth Heinemann, Oxford, England, U.K., 2004, pp. 500–503.

[15]Myers, R. H., and Montgomery, D. C., "Response Surface Methodology: Process and Product Optimization Using Designed Experiments," Wiley, New York, 1995.

[16]Vanderplaats, G. N., and Hanse, S. R., "DOT Users Manual," Ver. 5.0, Vanderplaats Research and Development, Inc. Colorado Springs, CO, Jan. 1999.

[17]Lee, B.-S., and Lee, D., "Data Parallel Symmetric Gauss–Seidel Algorithm for Efficient Distributed Computing, Using Massively Parallel Supercomputers," AIAA Paper 97-2138, July 1997.

[18]Kim, T.-Y., Lee, B.-S., and Lee, D.-H., "Study On Unsteady Wakes Behind a Square Cylinder Near a Wall," *Journal of Mechanical Science and Technology*, Vol. 19, No. 5, 2005, pp. 1169–1181.

[19]McCroskey, W. J., McAlister, K., Carr, L. W., and Pucci, S. L., "An Experimental Study of Dynamic Stall on Advanced Airfoil Sections" NASA TM 84245, Vol. 2, 1982, p. 146.

[20]Bousman, W. G., "Evaluation of Airfoil Dynamic Stall Characteristics for Maneuverability," *Proceedings of the 26th European Rotorcraft Forum*, Sept. 2000, Chap. 38, pp. 1–21.

[21]Giunta, A. A., "Aircraft Multidisciplinary Design Optimization Using Design of Experiments Theory And Response Surface Modeling Methods," Ph.D. Dissertation, Dept. of Aerospace Engineering, Virginia Polytechnic Inst. and State Univ., Blacksburg, VA, May 1997.